Sensitivity-enhanced solid-state NMR detection of expansin's target in plant cell walls

Tuo Wang[a], Yong Bum Park[b], Marc A. Caporini[c], Melanie Rosay[c], Linghao Zhong[d], Daniel J. Cosgrove[b,1], and Mei Hong[a,1]

[a]Department of Chemistry and Ames Laboratory, Iowa State University, Ames, IA 50011; [b]Department of Biology, Pennsylvania State University, University Park, PA 16802; [c]Bruker Biospin Corporation, Billerica, MA 01821; and [d]Department of Chemistry, Pennsylvania State University, Mont Alto, PA 17237

Contributed by Daniel J. Cosgrove, August 29, 2013 (sent for review July 29, 2013)

Structure determination of protein binding to noncrystalline macromolecular assemblies such as plant cell walls (CWs) poses a significant structural biology challenge. CWs are loosened during growth by expansin proteins, which weaken the noncovalent network formed by cellulose, hemicellulose, and pectins, but the CW target of expansins has remained elusive because of the minute amount of the protein required for activity and the complex nature of the CW. Using solid-state NMR spectroscopy, combined with sensitivity-enhancing dynamic nuclear polarization (DNP) and differential isotopic labeling of expansin and polysaccharides, we have now determined the functional binding target of expansin in the *Arabidopsis thaliana* CW. By transferring the electron polarization of a biradical dopant to the nuclei, DNP allowed selective detection of ^{13}C spin diffusion from trace concentrations of ^{13}C, ^{15}N-labeled expansin in the CW to nearby polysaccharides. From the spin diffusion data of wild-type and mutant expansins, we conclude that to loosen the CW, expansin binds highly specific cellulose domains enriched in xyloglucan, whereas more abundant binding to pectins is unrelated to activity. Molecular dynamics simulations indicate short ^{13}C-^{13}C distances of 4–6 Å between a hydrophobic surface of the cellulose microfibril and an aromatic motif on the expansin surface, consistent with the observed NMR signals. DNP-enhanced 2D ^{13}C correlation spectra further reveal that the expansin-bound cellulose has altered conformation and is enriched in xyloglucan, thus providing unique insight into the mechanism of CW loosening. DNP-enhanced NMR provides a powerful, generalizable approach for investigating protein binding to complex macromolecular targets.

carbohydrate-binding module | CBM

As part of the cell growth process, plants use expansins to induce wall stress relaxation, which creates the driving force for cell water uptake and consequent enlargement (1). Expansins were first discovered in studies of acid-stimulated growth of plant cells (2). Auxin, the classical plant growth hormone, rapidly stimulates growth in part by activating plasma membrane H^+-ATPases, lowering wall pH, thereby activating expansins, which have a low pH optimum. Expansins mediate wall loosening not by lysis of the major polysaccharides of the growing cell wall (CW), but by weakening the noncovalent polysaccharide network that constitutes the load-bearing structure of the CW (3).

Structural studies of the mechanism of expansin-mediated wall loosening have been hampered by the fact that active plant expansins are difficult to produce in recombinant expression systems. This obstacle was recently circumvented with the discovery of microbial expansins, which are readily expressed in *Escherichia coli* and enabled mutagenesis studies of the residues required for wall loosening and X-ray analysis of protein-oligosaccharide structures (4–6). These studies showed that expansins consist of two domains, D1 and D2, which present a nearly flat surface for binding to cellohexaose and related oligosaccharides. Mutagenesis and functional assays indicate that two distinct regions of the D2 domain have carbohydrate-binding properties: three conserved and linearly arranged aromatic residues on a hydrophobic surface of D2—resembling a type-A carbohydrate-binding module—are required for binding to pure microcrystalline cellulose and for wall loosening, whereas several nonconserved basic residues on the opposite side of D2 increase binding to whole CWs but do not promote wall loosening (5, 6).

Although we now know expansin's structure in atomic detail, its exact site of action in the native plant CW has not been structurally characterized because of the disordered and insoluble nature of CW polysaccharides and the fact that the only assays for expansin activity are biophysical, not biochemical. An attractive approach to this problem is solid-state NMR (SSNMR) spectroscopy, which can probe the structure of insoluble biomolecular complexes through intermolecular magnetization transfer, or spin diffusion (7–9). Two challenges in applying SSNMR to plant CWs are the overlapping ^{13}C signals of multiple polysaccharides (10, 11) and the trace amount (~0.1 wt% of the CW) of expansin at which it is operative (12). Using excess expansin to increase the detection sensitivity causes nonspecific binding, which complicates structural analysis. We recently overcame the first challenge by ^{13}C labeling of entire *Arabidopsis thaliana* plants (13), which enabled the use of 2D and 3D magic-angle-spinning (MAS) NMR techniques to resolve and assign the ^{13}C signals of various wall polysaccharides (14). To overcome the second challenge, we now use dynamic nuclear polarization (DNP), which enhances the NMR sensitivity by as much as two orders of magnitude by transferring the electron polarization of paramagnetic dopants to nuclear spins under microwave (MW) irradiation (15, 16). We show that DNP sufficiently enhanced the NMR sensitivity to allow determination of the functional binding target of EXLX1, a bacterial expansin from *Bacillus subtilis* (5). Furthermore, distinct

Significance

The protein expansin loosens the cell walls of plants for cell growth, but its carbohydrate target of binding has been elusive because of the difficulty of studying the noncrystalline plant cell wall by most structural biology techniques and the trace amount of expansin needed for wall loosening. We have now combined dynamic nuclear polarization sensitivity-enhanced solid-state NMR spectroscopy with ^{13}C labeling of *Arabidopsis thaliana* plants and ^{13}C, ^{15}N labeling of expansin, to determine that expansin binds cellulose microfibrils to loosen the plant cell wall. The expansin binding site is enriched in the hemicellulose xyloglucan and has a different cellulose structure from bulk cellulose, shedding light on the mechanism of wall loosening.

Author contributions: D.J.C. and M.H. designed research; T.W., Y.B.P., M.A.C., M.R., L.Z., and M.H. performed research; T.W., Y.B.P., D.J.C., and M.H. analyzed data; and T.W., D.J.C., and M.H. wrote the paper.

The authors declare no conflict of interest.

[1]To whom correspondence may be addressed. E-mail: dcosgrove@psu.edu or mhong@iastate.edu.

This article contains supporting information online at www.pnas.org/lookup/suppl/doi:10.1073/pnas.1316290110/-/DCSupplemental.

structural features of expansin-bound polysaccharides are observed, shedding light on CW sites important for wall loosening and wall mechanics.

Results and Discussion

DNP Enhancement of CW Spectra. We produced ^{13}C-labeled *Arabidopsis* CW by growing whole plants in media containing ^{13}C-labeled glucose (13). Non-CW molecules such as lipids and intracellular proteins were removed by detergent and protease extraction, followed by partial extraction of matrix polysaccharides to reduce nonspecific expansin binding (*SI Appendix*, Table S1). The ^{13}C, ^{15}N-labeled expansin was expressed by *E. coli* grown in minimal media, mixed with never-dried CW at a mass ratio of ~1:60–100, and hydrated with partially deuterated glycerol/water solution containing TOTAPOL [1-(TEMPO-4-oxy)-3(TEMPO-4-amino)propan-2-ol] (17), a biradical that exhibits high DNP efficiency. Solvent deuteration directs the electron polarization to ^{1}H spins in the proteins and polysaccharides, whereas glycerol protects the CW structure and uniformly distributes the biradical at the cryogenic temperature (~100 K) of the DNP experiments. A 600-MHz NMR spectrometer equipped with a 395-GHz gyrotron for high-power MW irradiation was used for the experiments. Fig. 1*A* shows 1D ^{13}C cross-polarization (CP) MAS spectra of CW that contains wild-type (WT) expansin. The spectra are simpler than reported *Arabidopsis* CW spectra (13) because of the reduced amount of pectins in the wall (*SI Appendix*, Table S1).

Turning on the MW enhanced the spectral sensitivities 27-fold (Fig. 1*A*). Low temperature and the presence of the biradical did not cause significant line broadening, based on comparisons with the ^{13}C linewidths of radical-free samples at high temperature (*SI Appendix*, Fig. S1) (18). Thus, the structural order of cellulose microfibrils in the plant CW is preserved at ~100 K, similar to pure microcrystalline cellulose (19). Moreover, the DNP-enhanced spectral pattern is similar to the high-temperature spectra (Fig. 1*A*), and the ^{1}H T_1 relaxation times are uniform for all carbons (*SI Appendix*, Table S2). This result demonstrates uniform transfer of the electron polarization to wall polysaccharides. These favorable properties, also seen for two other expansin-containing CW samples (*SI Appendix*, Fig. S2), indicate that plant CWs are ideal targets for structural studies by DNP NMR (20–22).

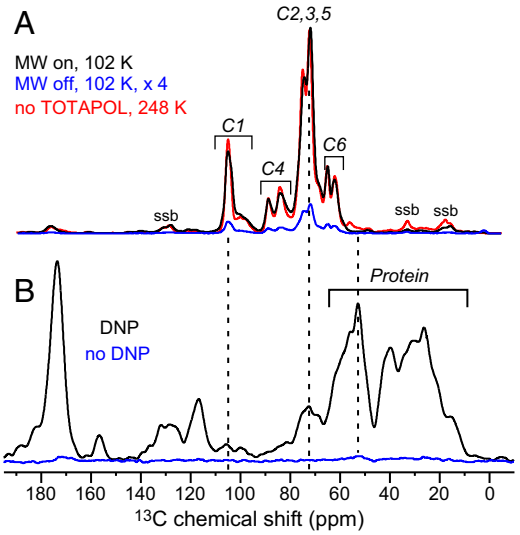

Fig. 1. The ^{13}C NMR spectra of *Arabidopsis* CW with WT expansin. (*A*) The ^{13}C CP-MAS spectra with MW on (black) and off (blue) at 102 K, showing 27-fold sensitivity enhancement. The DNP-enhanced spectrum has a similar pattern as the 248-K spectrum of a radical-free CW sample (red), indicating uniform sensitivity enhancement. ssb, MAS sidebands. (*B*) The ^{15}N-^{13}C filtered ^{13}C spectra after 1-s spin diffusion. Without DNP at 248 K (blue), little intensity was observed after 22,528 scans. With DNP at 102 K (black), strong protein and polysaccharide intensities were detected after 2,560 scans.

Identifying CW Polysaccharides near Expansin. To identify the target site of expansin in the CW, we exploited the fact that ^{15}N labels are present only in expansin and not in any CW biopolymers, by selecting the ^{13}C magnetization of expansin carbons that are directly bonded to nitrogens using a ^{15}N-^{13}C dipolar filter (*SI Appendix*, Fig. S3). Magnetization of the nitrogen-proximal ^{13}C spins was then transferred to the nearby polysaccharides through distance-dependent ^{13}C spin diffusion. Such protein-transferred ^{13}C spectra could not be observed without DNP because of the low amount of expansins (<0.23 mg) in these samples (Fig. 1*B*) and the unavoidable dilution of the protein ^{13}C magnetization among the more abundant CW polysaccharides. However, with DNP, strong protein ^{13}C signals were observed in the aliphatic (10–60 ppm), aromatic (120–160 ppm), and carbonyl (170–185 ppm) regions (Fig. 1*B*). Moreover, characteristic polysaccharide signals at 70–110 ppm became evident after >0.5 s of mixing, i.e., as expansin ^{13}C magnetization diffused to nearby polysaccharides. A 2D ^{13}C spectrum that directly correlates protein Cα and polysaccharide signals (*SI Appendix*, Fig. S4) confirmed that the polysaccharide intensities in the 1D spectra result from spin diffusion from expansin.

To compare the proximities of different polysaccharides to expansin and, thereby, determine the makeup of the functional binding site, we measured the protein-transferred ^{13}C spectra of the polysaccharides as a function of spin diffusion mixing time (Fig. 2) and compared CWs that contain WT expansin, a WWY mutant, or an RKK mutant (4). The WWY mutant (W125A/W126A/Y157A) replaces the three aromatic residues on the cellohexaose-binding D2 surface with Ala (5). The RKK mutant (R173Q/K180Q/K183Q) replaces three basic residues on the opposite surface of D2 with the uncharged Gln. The RKK mutant has stronger wall loosening activities than WT expansin, an effect that was postulated to result from reduction of nonspecific interactions of the basic protein with acidic pectins. All three samples show increasing polysaccharide intensities with mixing time (Fig. 2*A* and *SI Appendix*, Fig. S5), as expected for spin diffusion measurements. However, even after 3 s, the WT and the WWY spectra still show much lower interior cellulose C4 intensity at 89 ppm than in the equilibrium CP spectrum, indicating that neither the WT nor the WWY protein has equilibrated its magnetization with the cellulose microfibril. In contrast, the RKK mutant displayed a significantly higher 89-ppm peak (Fig. 2*B*), and the polysaccharide intensity envelope is closer to that of the CP spectrum, indicating closer average proximity to cellulose. Relative to the 52-ppm protein Cα signal, both the interior cellulose C4 peak at 89 ppm and the dominant polysaccharide 72-ppm peak increase in intensity in the order of WWY ≤ WT << RKK (Fig. 2*C*). Because the WWY mutant lacks wall-loosening activity while the RKK mutant is hyperactive, this trend in intensity strongly suggests that cellulose is the functional binding target of expansins and that the hyperactive RKK mutant binds cellulose with the shortest average distances. The short average distances may be due to short nearest-neighbor distances of RKK expansin to the cellulose microfibril, more RKK expansin bound specifically to the microfibril, or a combination of both.

Quantitative intensity analysis of the 3-s spin diffusion spectra relative to the equilibrium CP spectra (Fig. 2*D*) and spin diffusion buildup with time (Fig. 2 *E* and *F* and *SI Appendix*, Fig. S6) confirm that the RKK mutant brings interior cellulose closest to its equilibrium magnetization, whereas the WWY mutant transfers the least magnetization to cellulose. Moreover, among the three

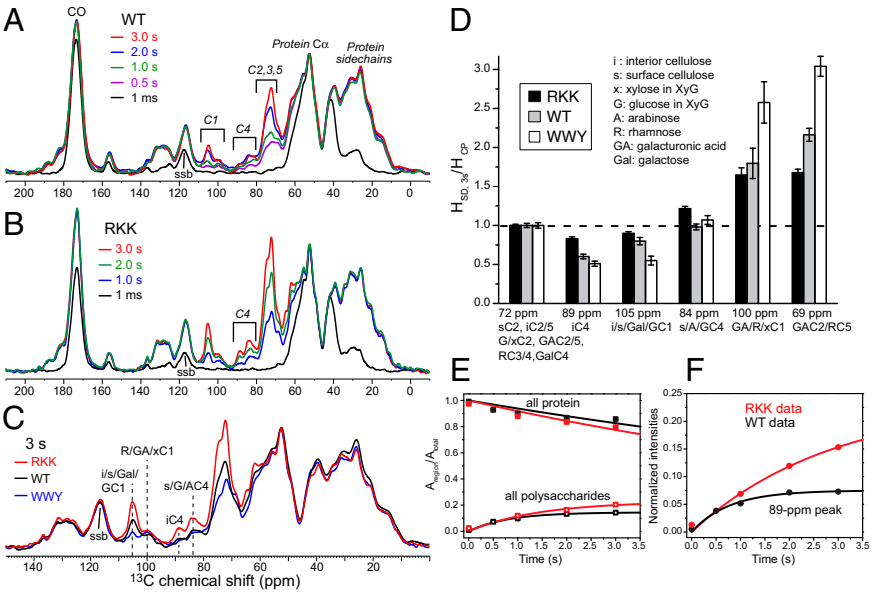

Fig. 2. DNP-enhanced ^{13}C spin diffusion spectra of expansin-bound CWs. (*A*) Spectra of CW that contains WT expansin after 1-ms to 3-s spin diffusion. (*B*) Spectra of CW that contains RKK-expansin after 1-ms to 3-s spin diffusion. (*C*) Three-second spin diffusion spectra of CWs with RKK, WT, and WWY expansins. Normalized to the protein Cα intensity, the RKK mutant shows the highest cellulose intensities. (*D*) Peak height ratios between the 3-s spin diffusion spectra and CP spectra, normalized to the 72-ppm intensity ratio. The RKK expansin has the highest iC4 intensity (89 ppm), whereas the WWY mutant has the highest pectin intensities (69 and 100 ppm). Polysaccharide abbreviations are indicated. (*E*) Decay of the total protein intensities (filled squares) and buildup of the total polysaccharide intensities (open squares) with time. RKK expansin (red) shows overall more spin diffusion transfer than WT expansin (black). (*F*) Intensity buildup of the 89-ppm peak of interior cellulose C4. The *y* axis plots the peak height ratio to the total intensity, further normalized by the ratio of the 72-ppm peak of the RKK sample at 3-s spin diffusion.

expansins, the WWY mutant has the highest magnetization transfer to pectins, indicating that weakening the aromatic interaction while preserving the basic residues favor expansin binding to pectins. This result is consistent with WWY's ability to bind whole CWs, which, however, does not cause wall loosening because cellulose binding is weakened (5).

Comparison with Computational Results. Molecular dynamics simulations of the expansin protein docked onto a cellulose microfibril (Fig. 3) verify the presence of atomic contacts between expansin and cellulose indicated by the spin diffusion NMR data. These simulations modeled cellulose as the I_β crystalline allomorph, which is the dominant form in plant CWs (23, 24) and used the crystalline structure of expansin complexed with cellohexaose (5) to guide the placement of the protein on the complex microfibril surface. The protein lies with its aromatic-triplet surface parallel to the edge of the hydrophobic (100) surface of the cellulose microfibril. The axis through the aromatic triplet is roughly parallel to the glucan axis, maximizing hydrophobic interactions. The shortest ^{13}C-^{13}C distances between the three aromatic rings and the pyranose rings are 4–6 Å, suggesting CH–π interactions. Similarly, the surface glucans are separated from the first layer of interior crystalline glucans by 4.2–5.4 Å. These distances are fully within ^{13}C spin diffusion reach, consistent with the observed 89-ppm peak of interior cellulose in the RKK spectra.

Distinctive Characteristics of the Expansin Binding Site. More detailed structure information about the expansin-bound region of the cellulose microfibril is obtained from a protein-transferred

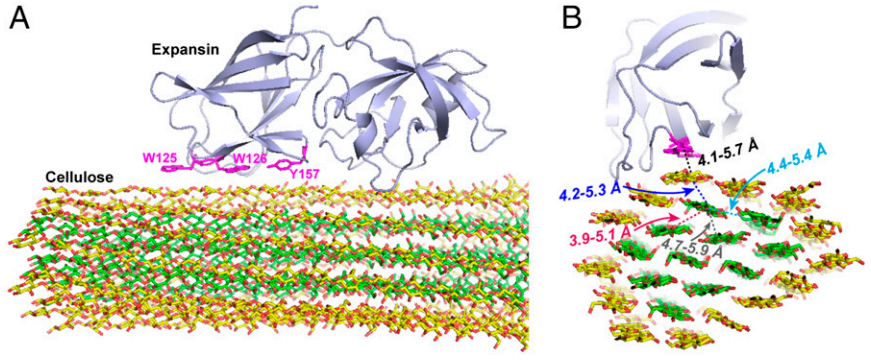

Fig. 3. MD simulation of expansin docking onto a cellulose I_β microfibril. (*A*) Side view showing the three aromatic residues (magenta) that bind to the (100) surface of the microfibril. Surface and interior cellulose carbons are colored in yellow and green, respectively. (*B*) Top view showing the shortest ^{13}C-^{13}C distances (4–6 Å) between expansin and the microfibril, and between surface and interior glucan chains. These short distances explain the protein-polysaccharide spin diffusion seen in the 1D and 2D ^{13}C spectra.

2D ^{13}C correlation spectrum of the RKK-expansin sample, whereby only cross-peaks of polysaccharides in close contact to the protein are detected (Fig. 4*A*). Several changes from the spin–diffusion-free 2D spectrum are observed. In the 99-ppm cross-section of xylose, galacturonic acid, and rhamnose C1, the cross-peak at 68 ppm (from galacturonic acid C1–C2 and rhamnose C1–C5) is weakened relative to the xylose C1-C2 cross-peak at 72 ppm (Fig. 4 *B–D* and *SI Appendix*, Fig. S7). This preferential enhancement of xylose intensities is also observed at several other cross-sections (*SI Appendix*, Fig. S7) and indicates that the expansin-bound site has higher XyG content and lower pectin content than the average CW. These results are reinforced by the spin diffusion 2D spectrum showing a cross-peak between the C1 of xylose and a Trp or Tyr aromatic carbon (*SI Appendix*, Fig. S8), which is consistent with atomic contact between the aromatic triplet (W125/W126/Y157) in the expansin protein and XyG-enriched regions of the cellulose microfibril.

Along with XyG enrichment, there is evidence that the expansin-bound interior cellulose has a C4 chemical shift that is 1-ppm lower than the average C4 frequency (compare yellow highlighted region in Fig. 4*B* with Fig. 4*C*). Because the C4 chemical shift is sensitive to the χ torsion angle around the C5–C6 bond, the lower shift suggests that the expansin binding site has a slightly altered interior cellulose conformation from that of the majority of cellulose. This change in cellulose conformation may be related to the presence of XyG near the expansin binding site: XyG is apparently able to modify cellulose crystallization during microfibril formation in model systems (25, 26). Another possibility is that expansin binding itself modifies the cellulose conformation, but the molecular dynamics simulation (above) gave no hint of such an effect.

These results demonstrate that expansin's potency for CW loosening coincides with its selective binding to a specific and quantitatively minor site in the CW comprised of a slightly altered cellulose conformation in close proximity to XyG. This conclusion extends and deepens inferences from competitive binding studies (5) showing that the cellulose binding site for expansin is distinct from and less abundant than that for a series of cellulose binding modules that bind to the crystalline surface or disordered regions of cellulose. Those studies, which were based on binding isotherms, were made with pure cellulose (Avicel and bacterial cellulose) to avoid masking by the dominant but unproductive binding of expansin to acidic polysaccharides in the more complex plant CW. DNP-enhanced NMR, in combination with the use of expansin mutants, was able to circumvent this problem in a more informative manner, to reveal unprecedented details about expansin's target for CW loosening.

One limitation of the current study stems from the use of the bacterial expansin, EXLX1, which is less active in wall-loosening assays than are plant expansins (4). This limitation stems from the difficulty of expressing plant expansins heterologously, which is a precondition for producing the labeled and mutated versions of expansin needed for our analysis. Because EXLX1 is homologous to plant expansins (4) and induces CW extension with characteristics very similar (although diminished) to plant expansins yet different from other wall loosening mechanisms (1, 27), we expect them to share the same target (see below as well), but verification of this point will require further testing.

Implications for CW Structure and Growth. These results with EXLX1 dovetail nicely with other recent studies that are leading to revisions in our concepts of primary CW structure in plants, particularly with respect to the prevalent notion that XyGs function as tethers to link microfibrils into a load-bearing network (3, 28, 29). For instance, analysis of CW mechanical changes induced by substrate-specific endoglucanases (30) showed that most of the XyG in the CW was irrelevant to wall mechanics and that key mechanical junctions in the CW may be restricted to relatively few, inaccessible regions, dubbed "biomechanical hotspots," where XyG and cellulose may be closely intertwined. The expansin-bound sites characterized here seem to be likely candidates for these regions, an idea that gains support from the observation that CWs lacking XyG are substantially diminished in their response to expansin (31). The idea that the majority of XyG does not contribute to CW mechanics in a major way is likewise supported by the relatively minor morphological and biomechanical phenotype of a genetic mutant of *A. thaliana* deficient in XyG (31, 32). Additionally, recent SSNMR data suggest that XyG interaction with cellulose in the CW is more limited than previously conjectured and may occur more by entrapment within microfibrils or groups of microfibrils than by coating the microfibril surface (13). Our characterization of expansin's functional binding site is consistent with these emerging concepts of the structure of the growing CW and strengthen the concept that CW loosening by expansin and other wall-loosening agents may be restricted to limited, specific structures in the CW.

Finally, we note that the approach demonstrated here of DNP-enhanced NMR combined with tailored isotopic labeling is generally applicable to structure elucidation of protein binding to other macromolecular complexes such as cytoskeletons and extracellular matrices.

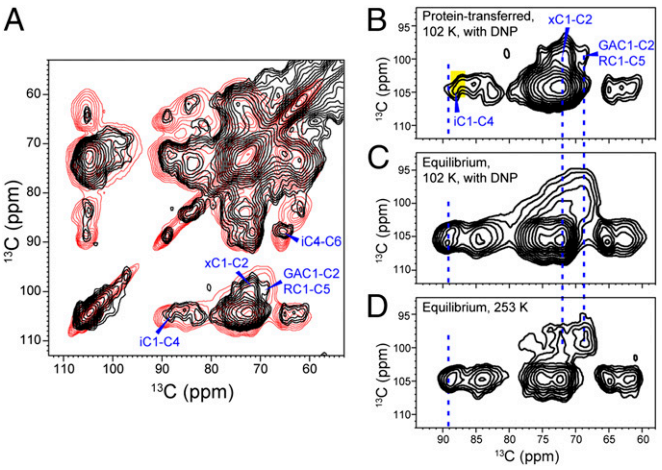

Fig. 4. Two-dimensional ^{13}C-^{13}C correlation spectra of RKK-bound CW polysaccharides. (*A*) DNP-enhanced 2D spectrum after 3-s intermolecular spin diffusion (black). Only polysaccharides in close contact with RKK-expansin are detected. The equilibrium 2D spectrum without spin diffusion is superimposed in red. (*B–D*) Comparison of the C1 region of several 2D spectra. (*B*) DNP-enhanced 3-s spin diffusion spectrum of the RKK CW sample at 102 K. (*C*) DNP-enhanced equilibrium 2D spectrum of the RKK CW sample at 102 K. (*D*) Equilibrium 2D spectrum of WT CW sample at 253 K without DNP (12). The spectrum in *B* has a higher xylose cross peak and a different iC4 chemical shift (highlighted in yellow) than the equilibrium spectra in *C* and *D*.

Materials and Methods

Protein and CW Samples. The ^{13}C, ^{15}N-labeled expansins (EXLX1 from *B. subtilis*) were expressed in *E. coli* and purified as described before (6), except that M9 minimal medium containing ^{13}C-labeled glucose and ^{15}N-labeled ammonium chloride were used as the only carbon and nitrogen sources. The ^{13}C-labeled CWs were produced by growing *A. thaliana* seedlings in the dark for 14 d in liquid medium containing 0.5% ^{13}C-glucose (13), followed by isolation and extraction of the CW without drying. The harvested seedlings were frozen and ground in liquid nitrogen, and the material was treated sequentially with 1.5% (wt/vol) SDS (3 h) to remove intracellular proteins, porcine pancreatic α-amylase (5,000 units in 30 mL of 50 mM Mes buffer at pH 6.8, 12 h at 37 °C) to remove starch, Pronase (200 units in 20 mL of MES

buffer at pH 7.5, 12 h at 40 °C) to further digest proteins, xyloglucanase [3 mg/mL from *Aspergillus aculeatus* (33) in 50 mM sodium acetate at pH 5.0], and 1 M NaOH with 20 mM $NaBH_4$ to reduce the amount of XyG and pectins. All solutions contained 0.02% NaN_3 to inhibit microbial growth, and multiple washes with deionized and distilled water were used between steps. The CWs were not dried or extracted with organic solvents to preserve native structure. Expansins were bound to the CW at a 1:100 ratio (dry mass) for the RKK and WWY samples and ∼1:60 for the WT sample. Expansin-bound CWs were centrifuged through a 40-μm filter to reach a water content of 40 wt%. Sugar composition analysis indicates that the resulting CWs contain 42% cellulose, 22% hemicellulose, and 36% pectin (*SI Appendix*, Table S1). The treatment with xyloglucanase and 1 M NaOH, which effectively enriched the CW cellulose content by removing 75% of the pectin and hemicellulose, would not be expected to alter cellulose structure or to dissociate tightly held complexes of cellulose and matrix polymers (28, 30).

For DNP experiments, the above CW samples were switched to a solution of 40% d_8-glycerol/D_2O/H_2O solution containing 35 mM TOTAPOL. A 43 mM stock solution of TOTAPOL was first prepared by dissolving 0.87 mg of TOTAPOL in 50 μL of d_8-glycerol:D_2O:H_2O (61:29:10 volume ratio) solution. Twenty to twenty-five milligrams of 40%-hydrated and expansin-containing CW was slowly dehydrated to ∼13%, then rehydrated with the TOTAPOL stock solution to reach a final hydration level of 40% and a TOTAPOL concentration of 35 mM. The final volume ratio of d_8-glycerol:D_2O:H_2O was 50:38:12. The mixture was stirred thoroughly and packed into a 3.2 mm sapphire rotor. The three CW samples contained 0.14 mg of WWY and RKK expansins and 0.23 mg of WT expansin. A control CW sample without TOTAPOL and with 36 mg of CW and 0.36 mg of expansin was measured at high temperature without DNP. A second control sample of pure expansin without the CW was used to compare the pure-expansin spectra with the NC-filtered spectra of expansin-containing CWs.

CW Sugar Composition Analysis. The ^{13}C-labeled *Arabidopsis* walls (∼3 mg) for the DNP NMR experiments were treated with 1 mL of 2 M trifluoroacetic acid (TFA) at 121 °C for 1 h to hydrolyze the matrix polysaccharides. The supernatant was dried under airflow and resuspended in distilled deionized water (ddH_2O). The 2 M TFA insoluble residue (predominantly cellulose) was hydrolyzed with 1 mL of 72% H_2SO_4 at room temperature for 1 h. The slurry of 72% H_2SO_4 was diluted with ddH_2O to 2 M concentration, incubated at 100 °C for 2 h with frequent vortexing (every 15 min), and neutralized with ammonium hydroxide (NH_4OH). Sugar composition of hydrolysates was assessed by high-performance anion-exchange chromatography with pulsed amperometric detection analysis. Briefly, TFA and H_2SO_4 hydrolyzed samples were filtered through a 0.1-μm filter (Amicon), and monosaccharides were separated on a Dionex Carbo PA-20 column at a flow rate of 0.5 mL· min^{-1} with 0.1 M NaOH isocratic elution for the first 15 min and then with linear gradient elution for 20 min starting with 0.1 M NaOH to a final mixture of 0.1 M NaOH and 0.1 M sodium acetate (1:1. vol/vol) and detected with a pulsed amperometric detector.

SSNMR Experiments. All SSNMR spectra were measured at a magnetic field of 14.1 T, corresponding to ^1H and electron Larmor frequencies of 600 MHz and 395.18 GHz, respectively. Spectra without DNP were measured between 248 and 293 K, whereas DNP-enhanced spectra were measured at 102 K. The DNP-enhanced NMR experiments were carried out at Bruker Billerica laboratories on an Avance III SSNMR spectrometer equipped with a 3.2-mm triple-resonance low temperature MAS probe (34, 35). MW irradiation was generated by a second-harmonic gyrotron operating with a MW power of 9 W at the sample. The samples were spun at 8.5 kHz, and the temperature with MW on was calibrated by using KBr T_1 measurements (36). Non-DNP–enhanced experiments were conducted on an Avance II wide-bore SSNMR spectrometer. The ^{13}C chemical shifts were referenced to tetramethylsilane either externally through adamantane or through the ^1H chemical shift by using the ratio of the gyromagnetic ratios of ^1H and ^{13}C.

One-dimensional NC-filtered ^{13}C spin diffusion experiments were conducted on expansin-containing CWs. The ^{13}C magnetization was prepared with ramped ^1H-^{13}C CP. A ^{15}N-^{13}C REDOR pulse train (t_{mix}) of 1.9 ms, corresponding to 16 rotor periods, was used to select the Cα and CO signals of expansin and remove all CW ^{13}C signals (*SI Appendix*, Fig. S3*A*). A variable mixing time of up to 3 s transferred the protein ^{13}C magnetization to the neighboring polysaccharides. For the buildup curves in Fig. 2*F* and *SI Appendix*, Fig. S6, intensities were calculated as $[H_x(t)/A_{total}(t)]/[H_{72,RKK}(3\ s)/A_{total,RKK}(3\ s)]$.

For the RKK sample, a 2D protein-polysaccharide ^{13}C correlation spectrum was measured. A t_1 period after the ^{15}N-^{13}C REDOR period encoded the protein signals, which were correlated to the polysaccharide signals after a long mixing period of 3 s (*SI Appendix*, Fig. S3*B*). A 2D protein-edited polysaccharide-polysaccharide ^{13}C correlation spectrum was also measured by first transferring the NC-filtered protein ^{13}C magnetization to the polysaccharides with a 3-s mixing time, then correlating the polysaccharide signals with each other with a 30-ms mixing time (*SI Appendix*, Fig. S3*C*). Only polysaccharides in close contact with RKK expansin exhibit intramolecular cross-peaks in this 2D spectrum.

Molecular Dynamics Simulations. The initial model of the expansin–CW complex was built by superimposing the carbohydrate substrate in the crystal structure of the EXLX1–cellohexaose complex [Protein Data Bank (PDB) ID code: 4FER, chain B] (5) onto an edge glucan chain on the (100) face of a cellulose I_β microfibril, constructed from 25 chains, each 20 glucose units long, pr-equilibrated from its crystal structure (24) in water. We note that the number of chains in a cellulose microfibril and their arrangement (cross-sectional shape) are not well established at this time (37, 38); the configuration chosen here represents a somewhat arbitrary structure between the extremes of numbers of chains and shapes that are commonly postulated in current literature; these details of microfibril structure are unlikely to affect the conclusions drawn from this simulation. The initial configuration was selected because it produces the least steric clashes between the protein and the substrate, compared with choosing the other protein chain in the PDB, or other glucan chains in the microfibril. Counterions were added to allow for particle-mesh-Ewald summation (39, 40). This complex structure was placed in a 129 × 81 × 64 Å periodic water box and subjected to molecular dynamics for step-wise heating at 100, 200, and 300 K each for 20 ps, followed by 40 ps of equilibration. Finally, a 40-ns production trajectory at 300 K within the microcanonical NVE ensemble was collected for analysis. The CHARMM package (41) was used for calculations, in conjunction with force fields of CHARMM27 for the protein (with CMAP correction) (42, 43), C35 for cellulose (44), and TIP3 for water (45).

ACKNOWLEDGMENTS. We thank Edward Wagner for help in producing labeled protein. T.W. and M.H. acknowledge Department of Energy (DOE) Grant AL 10-501-117163, D.J.C. and L.Z. acknowledge DOE-Basic Energy Science (BES) Grant DE-FG02-84ER13179, and Y.B.P. was supported by US-DOE-BES-Energy Frontier Research Centers Award DE-SC0001090.

1. Cosgrove DJ (1997) Relaxation in a high-stress environment: The molecular bases of extensible cell walls and cell enlargement. *Plant Cell* 9(7):1031–1041.
2. McQueen-Mason S, Durachko DM, Cosgrove DJ (1992) Two endogenous proteins that induce cell wall extension in plants. *Plant Cell* 4:1425–1433.
3. Cosgrove DJ (2000) Loosening of plant cell walls by expansins. *Nature* 407(6802): 321–326.
4. Kerff F, et al. (2008) Crystal structure and activity of Bacillus subtilis YoaJ (EXLX1), a bacterial expansin that promotes root colonization. *Proc Natl Acad Sci USA* 105(44): 16876–16881.
5. Georgelis N, Yennawar NH, Cosgrove DJ (2012) Structural basis for entropy-driven cellulose binding by a type-A cellulose-binding module (CBM) and bacterial expansin. *Proc Natl Acad Sci USA* 109(37):14830–14835.
6. Georgelis N, Tabuchi A, Nikolaidis N, Cosgrove DJ (2011) Structure-function analysis of the bacterial expansin EXLX1. *J Biol Chem* 286(19):16814–16823.
7. VanderHart D (1987) Natural-abundance 13C-13C spin exchange in rigid crystalline organic solids. *J Magn Reson* 72:13–47.
8. Meier BH (1994) Polarization transfer and spin diffusion in a solid-state NMR. *Adv Magn Opt Reson* 18:1–115.
9. Cady SD, et al. (2010) Structure of the amantadine binding site of influenza M2 proton channels in lipid bilayers. *Nature* 463(7281):689–692.
10. Newman RH, Davies LM, Harris PJ (1996) Solid-state ^{13}C nuclear magnetic resonance characterization of cellulose in the cell walls of Arabidopsis thaliana leaves. *Plant Physiol* 111(2):475–485.
11. Renard CM, Jarvis MC (1999) A cross-polarization, magic-angle-spinning, 13C-nuclear-magnetic-resonance study of polysaccharides in sugar beet cell walls. *Plant Physiol* 119(4):1315–1322.
12. McQueen-Mason SJ, Cosgrove DJ (1995) Expansin mode of action on cell walls. Analysis of wall hydrolysis, stress relaxation, and binding. *Plant Physiol* 107(1):87–100.
13. Dick-Pérez M, et al. (2011) Structure and interactions of plant cell-wall polysaccharides by two- and three-dimensional magic-angle-spinning solid-state NMR. *Biochemistry* 50(6):989–1000.
14. Wang T, Zabotina O, Hong M (2012) Pectin-cellulose interactions in the Arabidopsis primary cell wall from two-dimensional magic-angle-spinning solid-state nuclear magnetic resonance. *Biochemistry* 51(49):9846–9856.
15. Maly T, et al. (2008) Dynamic nuclear polarization at high magnetic fields. *J Chem Phys* 128(5):052211.

16. Hu KN, Song C, Yu HH, Swager TM, Griffin RG (2008) High-frequency dynamic nuclear polarization using biradicals: A multifrequency EPR lineshape analysis. *J Chem Phys* 128(5):052302.
17. Song C, Hu KN, Joo CG, Swager TM, Griffin RG (2006) TOTAPOL: A biradical polarizing agent for dynamic nuclear polarization experiments in aqueous media. *J Am Chem Soc* 128(35):11385–11390.
18. Lesage A, Bardet M, Emsley L (1999) Through-bond carbon-carbon connectivities in disordered solids by NMR. *J Am Chem Soc* 121(47):10987–10993.
19. Takahashi H, et al. (2012) Rapid natural-abundance 2D 13C-13C correlation spectroscopy using dynamic nuclear polarization enhanced solid-state NMR and matrix-free sample preparation. *Angew Chem Int Ed Engl* 51(47):11766–11769.
20. Takahashi H, et al. (2013) Solid-state NMR on bacterial cells: Selective cell wall signal enhancement and resolution improvement using dynamic nuclear polarization. *J Am Chem Soc* 135(13):5105–5110.
21. Renault M, et al. (2012) Solid-state NMR spectroscopy on cellular preparations enhanced by dynamic nuclear polarization. *Angew Chem Int Ed Engl* 51(12):2998–3001.
22. Cegelski L, et al. (2010) Plant cell-wall cross-links by REDOR NMR spectroscopy. *J Am Chem Soc* 132(45):16052–16057.
23. Atalla RH, Vanderhart DL (1984) Native cellulose: A composite of two distinct crystalline forms. *Science* 223(4633):283–285.
24. Nishiyama Y, Langan P, Chanzy H (2002) Crystal structure and hydrogen-bonding system in cellulose Ibeta from synchrotron X-ray and neutron fiber diffraction. *J Am Chem Soc* 124(31):9074–9082.
25. Hackney JM, Atalla RH, VanderHart DL (1994) Modification of crystallinity and crystalline structure of Acetobacter xylinum cellulose in the presence of water-soluble beta-1,4-linked polysaccharides: 13C-NMR evidence. *Int J Biol Macromol* 16(4): 215–218.
26. Whitney SEC, et al. (2006) Effects of structural variation in xyloglucan polymers on interactions with bacterial cellulose. *Am J Bot* 93(10):1402–1414.
27. Yuan S, Wu Y, Cosgrove DJ (2001) A fungal endoglucanase with plant cell wall extension activity. *Plant Physiol* 127(1):324–333.
28. Pauly M, Albersheim P, Darvill A, York WS (1999) Molecular domains of the cellulose/xyloglucan network in the cell walls of higher plants. *Plant J* 20(6):629–639.
29. Somerville C, et al. (2004) Toward a systems approach to understanding plant cell walls. *Science* 306(5705):2206–2211.
30. Park YB, Cosgrove DJ (2012) A revised architecture of primary cell walls based on biomechanical changes induced by substrate-specific endoglucanases. *Plant Physiol* 158(4):1933–1943.
31. Park YB, Cosgrove DJ (2012) Changes in cell wall biomechanical properties in the xyloglucan-deficient *xxt1/xxt2* mutant of Arabidopsis. *Plant Physiol* 158(1):465–475.
32. Cavalier DM, et al. (2008) Disrupting two Arabidopsis thaliana xylosyltransferase genes results in plants deficient in xyloglucan, a major primary cell wall component. *Plant Cell* 20(6):1519–1537.
33. Pauly M, et al. (1999) A xyloglucan-specific endo-beta-1,4-glucanase from Aspergillus aculeatus: Expression cloning in yeast, purification and characterization of the recombinant enzyme. *Glycobiology* 9(1):93–100.
34. Rosay M, et al. (2010) Solid-state dynamic nuclear polarization at 263 GHz: Spectrometer design and experimental results. *Phys Chem Chem Phys* 12(22):5850–5860.
35. Sarkar R, et al. (2011) An NMR thermometer for cryogenic magic-angle spinning NMR: The spin-lattice relaxation of (127)I in cesium iodide. *J Magn Reson* 212(2): 460–463.
36. Thurber KR, Tycko R (2009) Measurement of sample temperatures under magic-angle spinning from the chemical shift and spin-lattice relaxation rate of 79Br in KBr powder. *J Magn Reson* 196(1):84–87.
37. Guerriero G, Fugelstad J, Bulone V (2010) What do we really know about cellulose biosynthesis in higher plants? *J Integr Plant Biol* 52(2):161–175.
38. Thomas LH, et al. (2013) Structure of cellulose microfibrils in primary cell walls from collenchyma. *Plant Physiol* 161(1):465–476.
39. Darden T, York DM, Pedersen LG (1993) Particle mesh Ewald - an N.Log(N) method for Ewald sums in large systems. *J Chem Phys* 98:10089–10092.
40. Essmann U, et al. (2013) A smooth particle mesh Ewald method. *J Chem Phys* 1003: 8577–8593.
41. Brooks BR, et al. (2009) CHARMM: The biomolecular simulation program. *J Comput Chem* 30(10):1545–1614.
42. Mackerell AD, Jr., Feig M, Brooks CL, 3rd (2004) Extending the treatment of backbone energetics in protein force fields: Limitations of gas-phase quantum mechanics in reproducing protein conformational distributions in molecular dynamics simulations. *J Comput Chem* 25(11):1400–1415.
43. MacKerell AD, et al. (1998) All-atom empirical potential for molecular modeling and dynamics studies of proteins. *J Phys Chem B* 102(18):3586–3616.
44. Guvench O, et al. (2008) Additive empirical force field for hexopyranose monosaccharides. *J Comput Chem* 29(15):2543–2564.
45. Jorgensen WL, et al. (1983) Comparison of simple potential functions for simulating liquid water. *J Chem Phys* 79(2):926–935.

Supporting Information

Sensitivity-Enhanced Solid-State NMR Detection of Expansin's Target in Plant Cell Walls

Tuo Wang[1], Yong Bum Park [2], Marc A. Caporini [3], Melanie Rosay[3], Linghao Zhong[4], Daniel J. Cosgrove [2], and Mei Hong[1]

1. Department of Chemistry and Ames Laboratory, Iowa State University, Ames, IA 50011

2. Department of Biology, Pennsylvania State University, University Park, PA 16802

3. Bruker Biospin Corporation, 15 Fortune Drive, Billerica, MA 01821

4. Department of Chemistry, Pennsylvania State University, Mont Alto, PA 17237

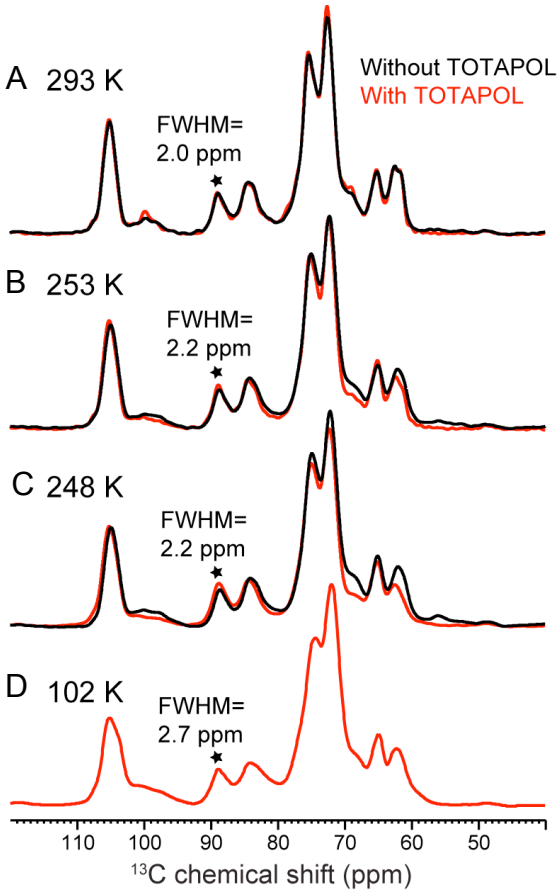

Figure S1. ^{13}C linewidths of WT-expansin containing CW as a function of temperature and radical. **A.** 293 K. **B.** 253 K. **C.** 248 K. **D.** 102 K. Spectra of the TOTAPOL-containing CW sample (red) have similar linewidths and intensity distributions as the spectra of CW without TOTAPOL (black), indicating that the biradical does not perturb the CW noticeably. Between 293 K and 248 K, the ^{13}C linewidth of the resolved 89-ppm peak of interior cellulose C4 is the same (2.0-2.2 ppm) within experimental uncertainty, while at 102 K, the C4 linewidth broadens moderately, to 2.7 ppm. Thus, the structural order of cellulose in the plant CW is largely preserved at low temperature, consistent with recent observations of microcrystalline cellulose (1).

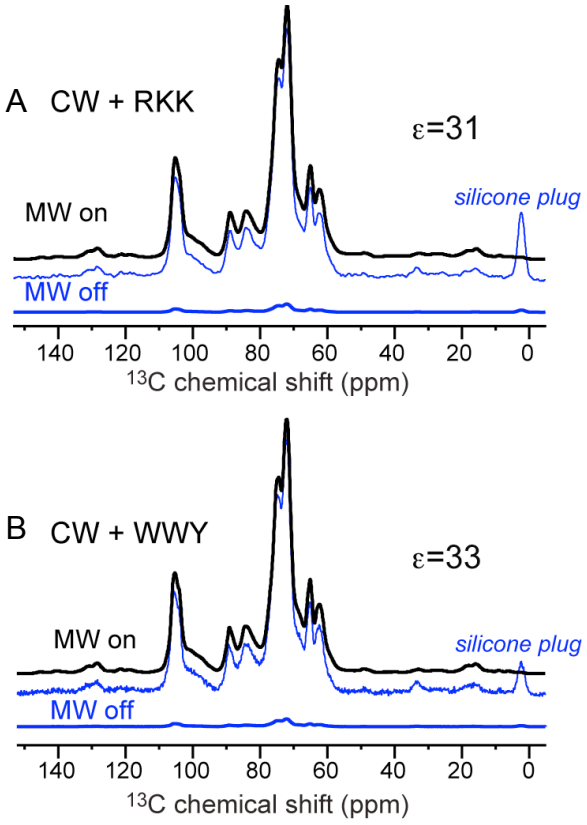

Figure S2. 1D ^{13}C CP-MAS spectra of *Arabidopsis* cell walls containing mutant expansins. **A.** CW with RKK expansin. **B.** CW with WWY expansin. Spectra measured with MW on (black) and off (blue) show the same intensity distributions, indicating uniform polarization transfer. Thin blue lines are the MW-off spectra scaled to the same maximum intensity as the MW-on spectra. The enhancement factors (ε) are 31 and 33. The signal near 0 ppm results from the silicone plug in the rotors.

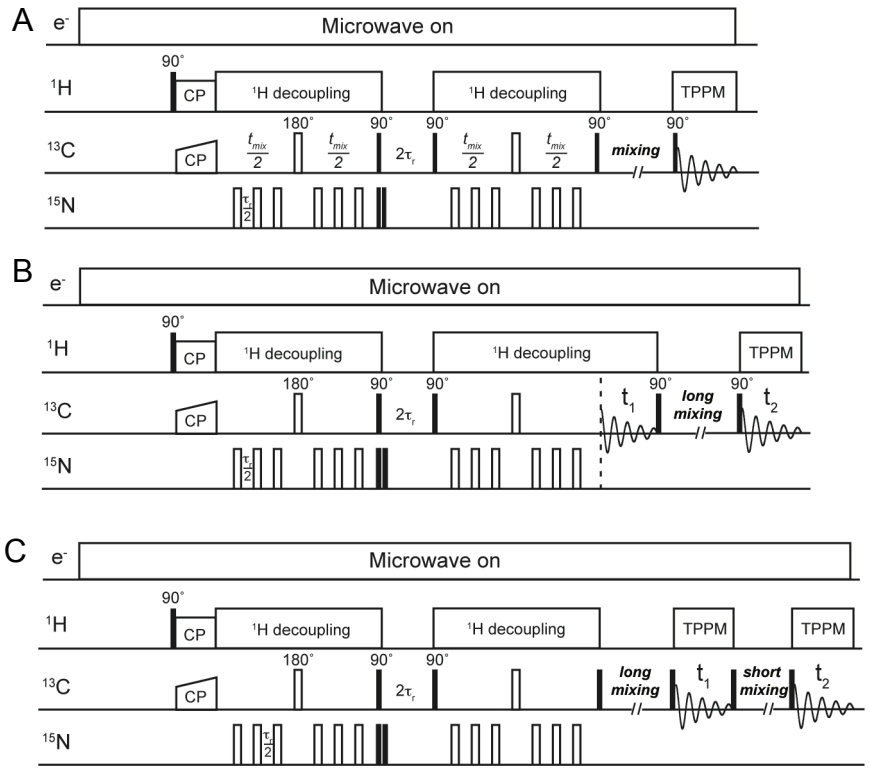

Figure S3. Pulse sequences used to determine the expansin binding target in the *Arabidopsis* cell wall. **A.** 1D NC-filtered ^{13}C spin diffusion experiment. ^{15}N-^{13}C REDOR (2) was used to select ^{13}C spins directly bonded to ^{15}N spins in the protein. The selected expansin ^{13}C magnetization is then allowed to transfer to polysaccharides during a mixing period. **B.** 2D protein-polysaccharide ^{13}C correlation experiment. ^{15}N-^{13}C REDOR selects the protein ^{13}C signals, which are encoded during the t_1 period and then correlated to the signals of neighboring polysaccharide ^{13}C spins after spin diffusion. **C.** Protein-edited polysaccharide-polysaccharide 2D ^{13}C correlation experiment. ^{15}N-^{13}C filtered protein ^{13}C magnetization is transferred to neighboring polysaccharides during a long mixing time, then intramolecular correlation of the ^{13}C magnetization is established using a short (30 ms) mixing time.

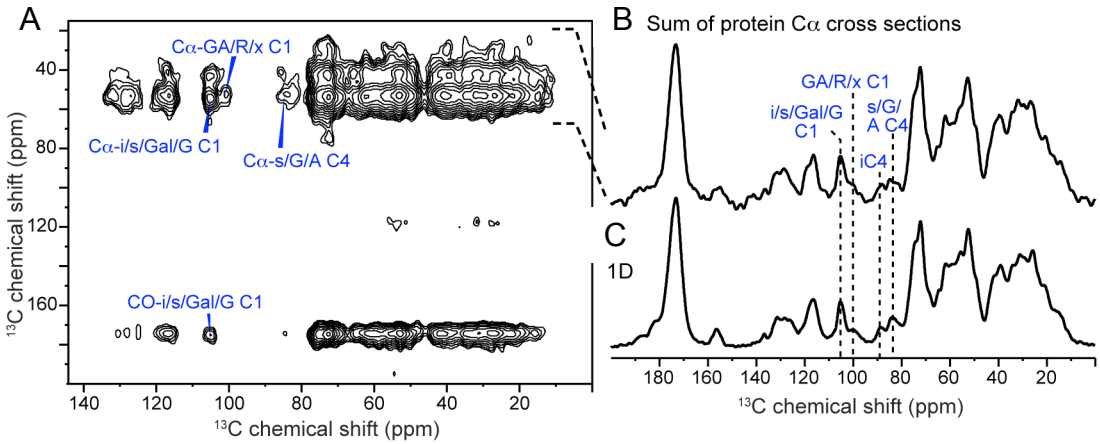

Figure S4. Direct evidence of protein-to-polysaccharide ^{13}C spin diffusion. **A.** DNP-enhanced 2D protein-polysaccharide ^{13}C correlation spectrum of cell wall containing bound RKK-expansin. The spectrum was measured with a 3 s mixing time between t_1 and t_2 periods. **B.** Sum of the ^{13}C cross sections between ω_1 frequencies of 20 and 68 ppm, which represent protein signals. **C.** 1D NC-filtered ^{13}C spin diffusion spectrum with a 3 s mixing time. The similarity of **B** and **C** confirms that the polysaccharide intensities in the 1D ^{13}C spin diffusion spectra result from magnetization transfer from expansin.

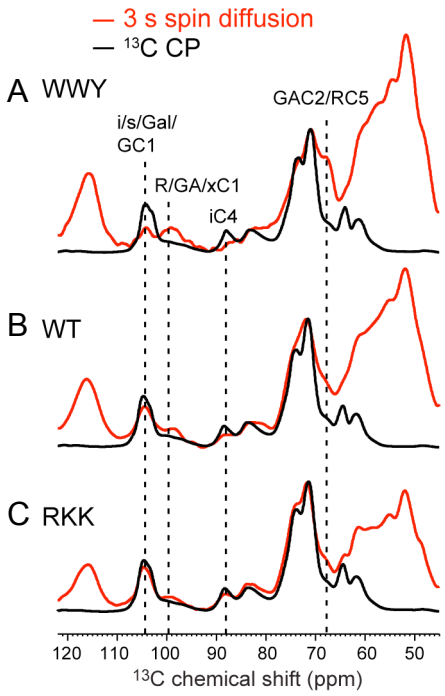

Figure S5. Comparison of DNP-enhanced 3 s ^{13}C spin diffusion spectra and ^{13}C CP spectra. **A.** CW with bound WWY-expansin. **B.** CW with bound wild-type expansin. **C.** CW with bound RKK-expansin. Each pair of spectra was scaled to match the maximum polysaccharide intensity at 72 ppm. Among the three expansins, the WWY mutant shows the lowest intensity for the 89-ppm interior cellulose C4 peak and the highest intensity for the pectin peaks at 100 ppm and 69 ppm. The RKK mutant has the opposite trend. These observations indicate that within the total magnetization transferred to the polysaccharides, the RKK mutant transfers more magnetization to cellulose than the other two expansins, while the WWY mutant transfers more magnetization to pectins than the other two expansins. The total magnetization transfer to all polysaccharides is the smallest by the WWY mutant and the largest by the RKK mutant, since the remaining intensities of the protein (below 65 ppm) are the lowest for the RKK mutant and the highest for the WWY mutant.

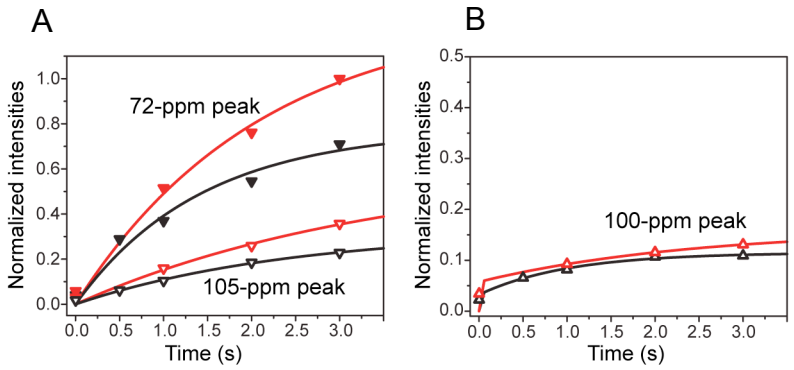

Figure S6. Protein-to-polysaccharide spin diffusion as a function of mixing time. WT expansin data (black) and RKK-expansin data (red) are compared. **A.** Buildup of the 72-ppm mixed C2/C3/C5 peak and the 105-ppm C1 peak, both dominated by cellulose. **B.** Buildup of the 100-ppm C1 peak of matrix polysaccharides galacturonic acid, rhamnose, and xylose. The y-axis plots the ratio of the peak height to the total spectral area, further normalized by the 72-ppm peak ratio of the RKK sample at 3 s spin diffusion. RKK expansin causes more magnetization transfer to cellulose than WT expansin, but similar magnetization transfer to pectins as WT expansin. Since the total transfer to polysaccharides is larger from RKK expansin (Fig. 2*E*) than from WT expansin, within the total magnetization transferred, a smaller fraction is transferred to pectins by RKK expansin than by WT expansin, consistent with the data in Fig. 2*D*. All buildup curves are fit with exponential functions as described before (3).

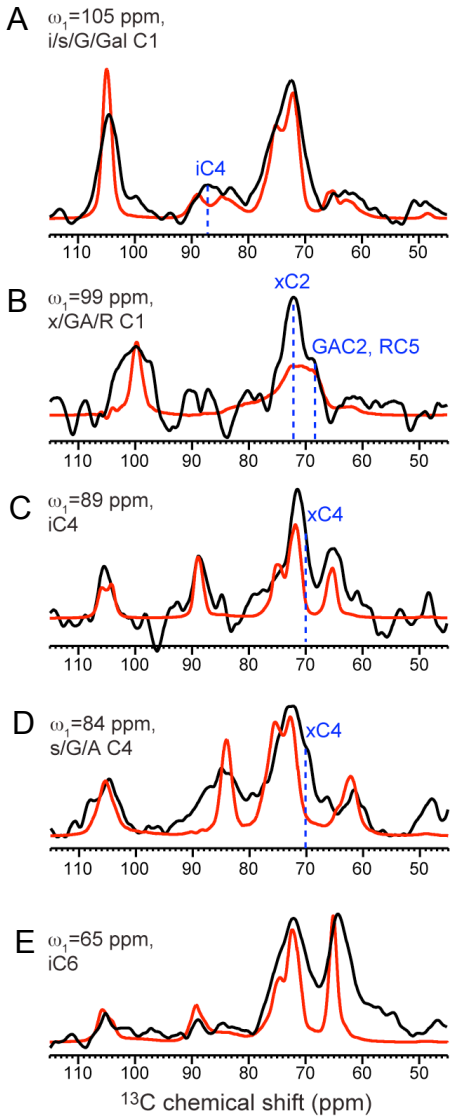

Figure S7. 1D cross sections of the protein-transferred (black) and equilibrium (red) 2D ^{13}C correlation spectra of the RKK-expansin bound CW sample. Both 2D spectra were measured at 102 K with DNP (Fig. 4). **A.** 105-ppm cross section of mixed C1 peaks. **B.** 99-ppm cross section of xylose, GalA, and Rha C1. The protein-transferred spectrum has higher xylose C2 peak than the GalA C2/Rha C5 peak, indicating that the expansin binding site is enriched in xyloglucan. **C.** 89-ppm cross section of interior cellulose C4. **D.** 84-ppm cross section of mixed C4 peaks. Both **C** and **D** show enhanced xylose C4 intensities at 70 ppm compared to the equilibrium spectra. **E.** 65-ppm cross section of interior cellulose C6.

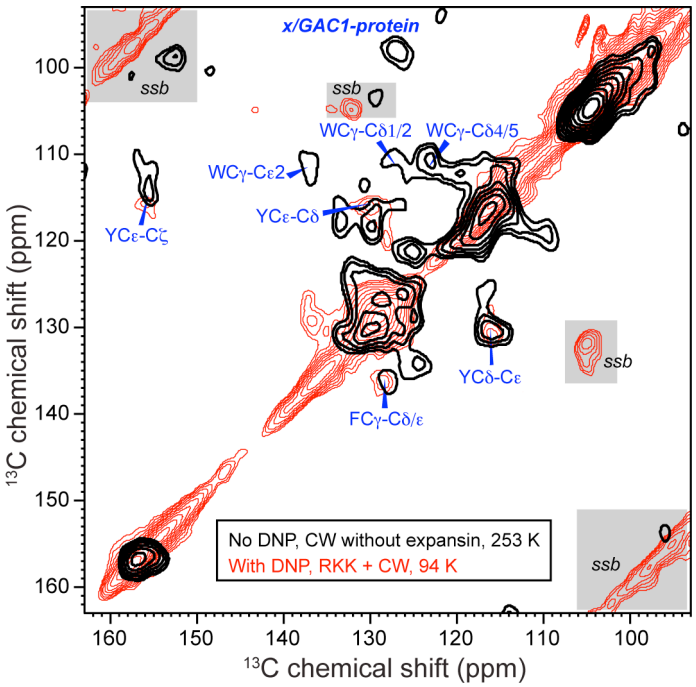

Figure S8. Aromatic region of the 2D ^{13}C correlation spectra of cell walls with and without spin diffusion from expansin. Black: DNP-enhanced protein-transferred 2D spectrum of the RKK-expansin bound CW. The protein-polysaccharide mixing time was 3 s. Red: 2D ^{13}C correlation spectrum of expansin-free CW, measured without DNP at 253 K on a 900 MHz NMR spectrometer (3). The DNP-enhanced 2D spectrum shows a protein-polysaccharide cross peak at (ω_1, ω_2) = (98, 127) ppm as well as intra-residue Trp, Tyr and Phe cross peaks. MAS spinning sidebands (ssb) are shaded.

Table S1. Monosaccharide composition of extracted and unextracted *Arabidopsis* cell walls.

Units: mole % based on total sugars (± SEM, $n = 2$ for unextracted (control) walls, 3 for extracted walls)

		Fuc	Rha	Ara	Gal	Glc	Xyl/Man*	GalA	GluA
2 M TFA	Control	1.9 (± 0.1)	7.4 (± 2.0)	16.0 (± 1.0)	15.7 (± 0.7)	11.9 (± 0.2)	15.4 (± 0.2)	13.9 (± 1.1)	0.8 (± 0.6)
	Extracted	1.9 (± 0.3)	5.0 (± 0.3)	10.8 (± 0.5)	14.5 (± 0.4)	4.3 (± 0.3)	12.9 (± 1.5)	4.9 (± 2.2)	1.4 (± 0.1)
H_2SO_4	Control	-	-	-	-	15.7 (± 1.4)	1.2 (± 0.1)	-	-
	Extracted	-	-	-	-	42.5 (± 0.3)	1.8 (± 0.5)	-	-

Estimated polysaccharide contents based on sugar analysis**

	Cellulose	Xyloglucan	Xylan + Mannan	Pectin
Control	15.7 %	24.0%	8.7 %	51.6 %
Extracted	42.5 %	8.6 %	13.1 %	35.8 %

*Our analysis did not distinguish xylose from mannose.

**Polysaccharide contents were estimated from sugar analysis as follows: Glc in the TFA-hydrolyzed fraction is assigned to xyloglucan with a saccharide composition Glc:Xyl:Gal:Fuc 1:0.75:0.16:0.10 (based on ref. (4)). After subtraction of the xyloglucan sugars, the residual Xyl/Man in the TFA-hydrolyzed fraction was assigned to arabinoxylan (Xyl:Ara 1:0.25) and mannan in a ratio of 2:1 (based on ref. (5)). The Xyl/Man in the H2SO4-hydrolyzed fraction was added to this number to estimate xylan + mannan. Hemicellulose is the sum of xyloglucan + xylan + mannan. All of the residual sugars (Gal, Ara, GalA, Rha, Fuc, GluA) were assigned to the pectin category. Glc in the H2SO4-hydrolyzed fraction was assigned to cellulose (the absence of Gal in this fraction indicated negligible xyloglucan content). The high cellulose content of the extracted wall, used in our analysis, is due to removal of 75% of the matrix polysaccharides by the extraction procedure.

Table S2. ^{1}H T_1 relaxation times of *Arabidopsis* cell walls at 102 K, measured using a ^{13}C-detected ^{1}H saturation recovery experiment.

^{13}C chemical shift	Assignment	^{1}H T_1 (s) with WT expansin	^{1}H T_1 (s) with RKK expansin	^{1}H T_1 (s) with WWY expansin
177 ppm	CO	8.7	3.6	7.5
105 ppm	i/s/Gal/GC1	8.9	3.7	8.2
100 ppm	GA/R/xC1	8.6	3.6	8.0
89 ppm	iC4	8.9	3.7	8.2
84 ppm	s/G/AC4	8.7	3.6	8.0
72 ppm	sC2, iC2/5, G/xC2, GAC2/5, RC3/4, GalC4	8.7	3.7	8.1
65 ppm	iC6	8.6	3.6	8.1
62 ppm	s/G/GalC6, A/xC5	8.7	3.6	8.1

Supporting References

1. Takahashi H, *et al*. (2012) Rapid natural-abundance 2D 13C-13C correlation spectroscopy using dynamic nuclear polarization enhanced solid-state NMR and matrix-free sample preparation. *Angew Chem Int Ed Engl* 51:11766-11769.
2. Gullion T & Schaefer J (1989) Rotational echo double resonance NMR. *J Magn Reson* 81:196-200.
3. Wang T, Zabotina O, & Hong M (2012) Pectin-cellulose interactions in the Arabidopsis primary cell wall from two-dimensional magic-angle-spinning solid-state nuclear magnetic resonance. *Biochemistry* 51(49):9846-9856.
4. Pena MJ, Ryden P, Madson M, Smith AC, & Carpita NC (2004) The galactose residues of xyloglucan are essential to maintain mechanical strength of the primary cell walls in Arabidopsis during growth. *Plant Physiol* 134(1):443-451.
5. Zablackis E, Huang J, Müller B, Darvill AG, & Albersheim P (1995) Characterization of the cell-wall polysaccharides of Arabidopsis thaliana leaves. *Plant Physiol* 107:1129-1138.